Pile Response to Horizontal Cyclic Loads

Masahiro SHIRATO*, Junichi KOSEKI†, and Jiro FUKUI‡

Abstract: This paper proposes a new hysteretic mechanism for Winkler type horizontal soil-foundation interaction springs for dynamic analyses of deep foundations. The experimental results of prototype piles subjected to cyclic lateral loading are reviewed. Plane strain test results of sand subjected to cyclic compression-extension loading are also investigated in order to account for the soil-pile load transfer mechanism from a theoretical point of view. These two investigations show that load transfer between soil and foundation depends on loading patterns. Numerical simulations using the proposed model show good agreement with the results of experiments on single piles subjected to fully reversed or one-sided horizontal cyclic loading.

INTRODUCTION

Due to the disastrous effects of earthquakes in past decades, the need for the use of dynamic analyses of foundations as well as structures in practical seismic design has been recognized. In practice, engineers often examine the soil-foundation interaction based on the beam-on-Winkler-foundation concept in pushover analysis. In the beam-on-Winkler-foundation concept, engineers model a pile (or deep foundation) as a beam and model the soil-pile load transfers as distributed springs along the length of the pile. The soil-pile load transfer of a Winkler spring at each depth is comprised of the relationship between the soil resistance per unit area p and the displacement y of the pile relative to the far-field soil at that depth, and this relationship is usually referred to as the p-y curve or p-y relation. However, some effort is required in order to plug a nonlinear hysteretic mechanism in the p-y relation beyond the static nonlinear pushover analysis into nonlinear dynamic analyses. Typical mechanisms such as the bi-linear mechanism and Masing's rule are often assumed, but most of these assumptions have not been verified.

This study explores a new model for the hysteretic mechanism of Winkler interaction springs between soil and foundation from a practical point of view. First, we observe the experimental results for piles embedded in sand and subjected to either fully reversed or one-sided cyclic loading at the top. These two loading patterns can be regarded as extreme cases of seismic random loading. Then, the characteristics of load transfer hystereses between soil and foundation are examined with respect to soil mechanics. We attempt to associate the behavior of sand subjected to cyclic compression and extension deformation in a soil element level with the load transfer hysteresis in the soil-pile interaction. In addition, we clarify the characteristics to be considered in the dynamic analyses for the soil-pile interaction based on these experimental and theoretical investigations and propose a new hysteretic mechanism of

*Senior Researcher, Foundation Engineering Research Team, Public Works Research Institute
†Professor, Institute of Industrial Science, University of Tokyo
‡Team Leader, Foundation Engineering Research Team, Public Works Research Institute

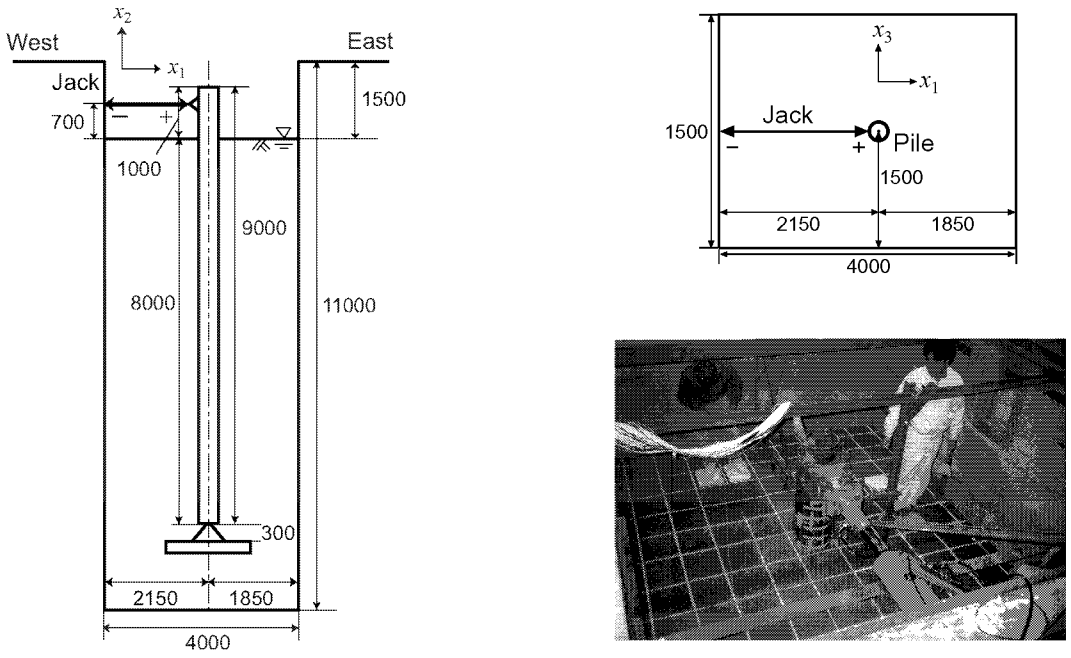

Figure 1 Test setup (units: mm)

interaction springs for random loading. Finally, we examine the accuracy and characteristics of the proposed hysteretic mechanism through simulation of piles embedded in sand and subjected to cyclic loading.

HORIZONTAL CYCLIC LOADING TESTS ON SINGLE PILES IN SAND

Test set-up

The experiment discussed herein was reported in detail by Fukui et al. (1998). **Figure 1** illustrates the experimental set-up.

The soil deposit was made of Kashima sand (D_{50} = 0.67 mm and U_c = 2.66) in a deep test pit at the Foundation Engineering Laboratory of the Public Works Research Institute. The deep test pit is 4 m long and 3 m wide in plan view, and has a depth of 11 m. The sand deposit was loose and saturated. The average relative density D_r and average dry density of the soil deposit estimated from core-cutter samples were 17% and 1.51 t/m^3. During each experiment, the water level was maintained at the ground surface level. An internal friction angle of 39 deg. was provided by a drained triaxial compression test conducted with D_r = 30% (ρ_d = 1.53 t/m^3) and σ'_c = 29.4 kN/m^2, where σ'_c is a confining stress. Cyclic triaxial compression tests provided a small strain shear modulus G_0 at a shear strain level on the order of 10^{-4} as:

$$G_0 = 1935(\sigma'_c/98)^{0.65} \times 98 \quad (\text{kN/m}^2), \tag{1}$$

where the unit of σ'_c is kN/m^2.

Steel pipe piles, each having a diameter of 318.5 mm and an embedded depth of 8 m, were used in the experiment. One pile had a wall thickness of 10.3 mm and was made of STK490, the other pile had a wall thickness of 5.6 mm and was made of STK400. We

Table 1 Results of material element tests for the steel pipe pile specimens

Specimen	Yield stress (N/mm^2)	Young's modulus (kN/mm^2)
SPP-1	562.0	228
SPP-2	589.1	238

Table 2 Experimental cases

Case	Cyclic loading pattern	Specimen
S1	Fully reversed	SPP-1
S2	Fully reversed	SPP-2
S3	One-sided	SPP-2

hereinafter refer to the former specimen as SPP-1 (Steel Pipe Pile 1) and the latter specimen as SPP-2. The material element test results on these piles are tabulated in **Table 1**. The point of application of the lateral cyclic loading was 0.7 m above the initial sand deposit surface (ground level). A pinned device was attached at the bottom of pile. Strain gauges were placed on the sides of pile that were orthogonal to the loading plane.

The experimental cases examined herein are listed in **Table 2**. In particular, the patterns of loading differed among the experimental cases. In Cases S1 and S2, the piles were subjected to reversed lateral displacement cycles at the load point of the specimen. The amplitude of the specified displacement was gradually increased from δ to $n \times \delta$ (n = 2, 3, 4, ...), where δ was 15 mm. In Case S3, one-sided lateral displacement cycles were applied. The amplitude of displacement was controlled in loading phases, and the load was then released simply in unloading phases in Case S3. This difference in the loading pattern is a noteworthy feature of these experiments, unlike most cyclic loading experiments that are performed only under reversed cyclic loading conditions. Hence, the present study more closely models seismic effects because it deals with two extreme cyclic load patterns in seismic random loading. The pile specimens used in each experimental case are listed in **Table 2**.

Observation of p-y curves

In the present study, p-y curves were derived from strain gauge data, where p is the soil resistance to the pile, in other words, the subgrade reaction intensity, and y is the relative displacement between the pile and the far field of the soil deposit. In these experiments, the soil displacement in the far-field is supposed to be zero. Shown in **Figure 2** are comparisons of p-y relationships among the experimental cases at a depth of 0.96 m below the ground level. Only the data measured when the pile bodies behaved elastically are shown in **Figure 2**. The solid lines correspond to the results for Cases S1 and S2, and the dotted lines correspond to the results for Case S3.

In the case of fully reversed cyclic loading, we have the following characteristics:

- A reloading path runs toward a point $|y|_{max}$ on the envelope curve on the opposite side, where $|y|_{max}$ corresponds to the ever-largest displacement.
- Unloading paths are stiffer than reloading paths, and the gradients of unloading paths do not seem to change significantly, even when $|y|_{max}$ is updated.

Note that the term 'reloading' refers to the case when the increment of $|p|$ is positive, and the term 'unloading' refers to the case when the increment of $|p|$ is negative. An 'envelope curve', denoted by a dashed line, is defined as a curve that is derived by connecting neighboring peak points of the first loops.

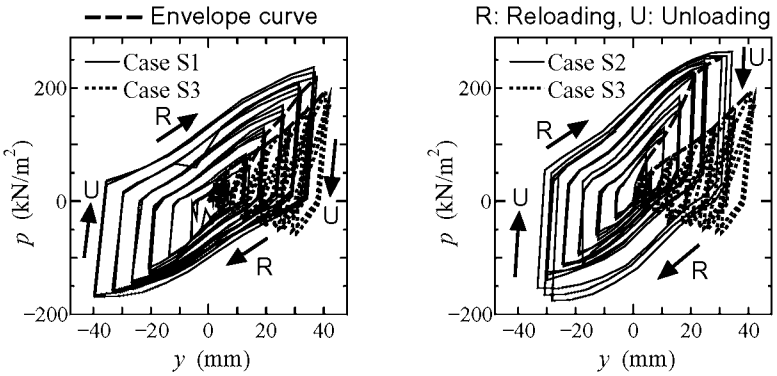

Figure 2 Comparison in *p*-*y* hysteresis among three experimental cases (GL −0.96 m)

In addition, **Figure 2** indicates that the mobilized soil resistances in the case of one-sided cyclic loading (Case S3) are smaller than those in the case of fully reversed cyclic loading (Cases S1 and S2) at the same displacement level. A similar tendency was also observed at different depths.

Figure 3 compares all of the envelope curves obtained in the experiments in the positive load and displacement region. The lateral load capacity of Case S3 was less than that of Case S2 in the pre-peak strength states, despite the fact that the pile specimen and soil conditions were identical. It should be noted that observation of the pile after the Case S2 experiment revealed that the pile failed at a depth of 1.55 m below ground level, and that the cross-section was badly distorted into a kind of oval shape with the short axis running parallel to the loading direction. As a consequence, postpeak behavior appeared.

EFFECTS OF STRESS-DILATANCY BEHAVIOR ON *p*-*y* RELATIONS

Review of the behavior of sand subjected to cyclic loading

During earthquakes, whilst the soil in the far-field of a foundation is primarily subjected to cyclic horizontal shear deformation, the soil in the near-field is primarily subjected to cyclic passive (compression) and active (extension) deformation due to the relative displacement between the pile and the far-field of the ground, as shown in **Figure 4**. In the same manner, the surrounding soil in the pile load experiment sustained cyclic compression-and-extension deformation. Therefore, consideration of the nonlinearity of soil in such a deformation mode in the near-field is likely to account for the load transfer characteristics of soil-pile interaction springs.

Masuda et al. (1999) performed a series of special plane strain tests on saturated specimens of air-pluviated Toyoura sand, to which cyclic compression and extension histories were applied. The sand specimen was under a consolidation condition, which models the overburden stress at a depth under ground, and was subjected to an axial deformation history. In addition, monotonic compression and extension tests were also performed under the same conditions.

A typical result from their tests is plotted in **Figure 5**. The major and minor principle stress axes are x_1 and x_2, respectively, and the x_1-direction corresponds to the horizontal

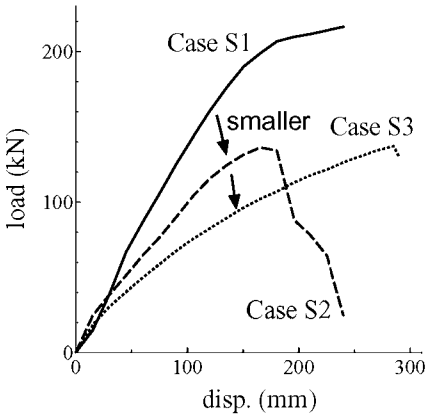

Figure 3 Envelope curves of load and displacement hystereses in the positive region at the load point for all experimental cases

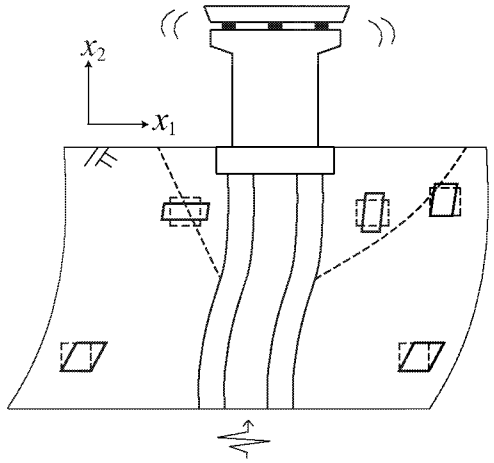

Figure 4 Deformation modes of soil in a soil-foundation system during an earthquake

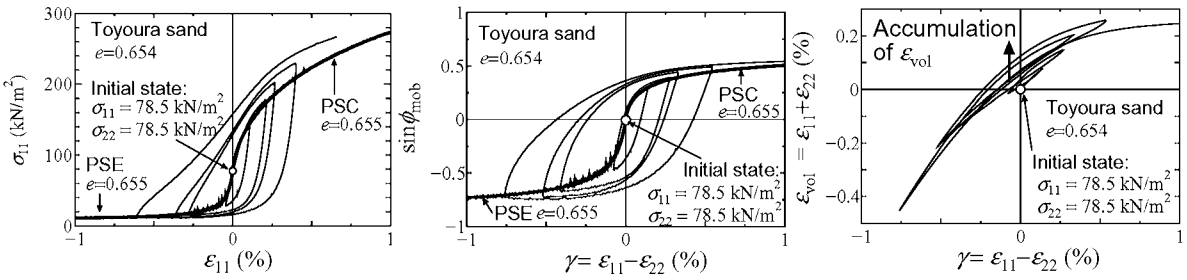

Figure 5 σ_{11}-ε_{11}, ε_{vol}-γ and $\sin\phi_{mob}$-γ relations obtained via a plane strain cyclic test and plane strain compression (PSC) and plane strain extension (PSE) tests of isotropically consolidated specimens of Toyoura sand, performed by Masuda et al. (1999)

direction in the field as illustrated in **Figure 4**. γ and ε_{vol} are shear and volumetric strains, respectively, and are defined as

$$\gamma = \varepsilon_{11} - \varepsilon_{22} \quad \text{and} \quad \varepsilon_{vol} = \varepsilon_{11} + \varepsilon_{22}, \tag{2}$$

in the plane strain condition. Changes in volume, i.e. increments of ε_{vol}, $\Delta\varepsilon_{vol}$, are negative for volume dilation and are positive for negative volume dilation, which is equivalent to volume contraction. In the test result, principal stresses and strains are considered to be positive in compression. ϕ_{mob} is the mobilized internal friction angle and is expressed by

$$\sin\phi_{mob} = \frac{R-1}{R+1}, \tag{3}$$

where R is the ratio of principal stresses $R = \sigma_{11}/\sigma_{22}$.

The left-hand graph in **Figure 5** shows the relationship between axial stress σ_{11} and axial strain ε_{11}. This relationship is indeed associated with the variation of the earth pressure coefficient. During the transition from a passive compression state to an active extension state, the soil resistance decreases steeply, and eventually a small resistance is maintained.

In contrast, during the transition from an extension state to a compression state, the soil resistance gradually increases toward the past peak point. When the soil-pile interaction at a depth under ground is simplified into a model comprised of an object sandwiched by two soil blocks, as shown in **Figure 6 (a)**, the superposition of the σ_{11}-ε_{11} relationship for one soil block plus the relationship of $(-\sigma_{11})$-$(-\varepsilon_{11})$ for the other soil block will form a hysteresis shape equivalent to the *p-y* relations observed in the reversed cyclic horizontal load experiments. In this manner, the element test result can indicate the *p-y* behavior.

The center and right-hand side graphs of **Figure 5** show a general expression of soil behavior involved with all principal stress and strain components. As the $\sin\phi_{mob}$-γ relationship indicates, the mobilized shear strength and shear strain has a typical hysteretic behavior under cyclic compression-extension loading, which can be expressed by a combination of a hyperbolic or exponential function for the skeleton curve and Masing's rule for the hysteretic mechanism, for example. This indicates that the mobilized shear strength of soil has a sort of unique relationship with shear strain when the soil is subjected to cyclic compression-extension loading.

On the other hand, the right-hand graph in **Figure 5** shows a shift of the ε_{vol}-γ curve with the increasing number of cycles and, as a result, the accumulation of negative dilatant deformation (volume contraction, i.e. the increment of ε_{vol} is positive) at every loading cycle. This fact, together with Eq. (2), reveals that strain components interact with each other and do not have a stationary relationship. This indicates that the evolution of strain components versus cyclic compression-extension loading can vary depending on the loading pattern. Therefore, the mobilized value of soil resistance ϕ_{mob} can also depend on the loading pattern. We can infer that the loading pattern dependency of *p-y* on piles is induced by the difference in the stress-dilatancy behavior of soil depending on the cyclic loading pattern.

Analytical investigation

An analytical investigation with respect to the element level of sand is performed in order to confirm the abovementioned assumption regarding the role of the stress-dilatancy characteristic of soil in the load pattern dependency of *p-y*. A simple analytical model, as illustrated in **Figure 6 (a)**, is adopted. A rigid body is sandwiched by plane strain sand blocks under a confined pressure. Horizontal displacement at both ends is fixed. We control only the horizontal displacement of the center rigid body, $y(t)$, and examine the response of soil resistance, $p(t)$, per unit area acting on the center rigid body at time t.

This models the state of a system consisting of a pile and the surrounding soil, and the system is sliced with a depth of dx_2. The rigid body and the plane strain sand blocks are regarded as a pile and an interaction zone between the pile and the far-field of the ground. The x_1-direction corresponds to the horizontal direction in the field.

This paper reports analytical results based on the assumptions described in the following. An isotropic consolidation condition is assumed. The skeleton curve (or monotonic loading curve) of the $\sin\phi_{mob}$-γ relation is assumed to be symmetric about the origin and is modeled by a hyperbolic curve. The material parameters used to describe the skeleton curve, assuming typical values, are as follows: the maximum mobilized internal friction angle ϕ_{max} is 30 deg. for giving the maximum value of $\sin\phi_{mob}$; the reference shear strain γ_r is 0.0002 for setting the initial tangent gradient of the skeleton curve, $\sin\phi_{max}/\gamma_r$. The hys-

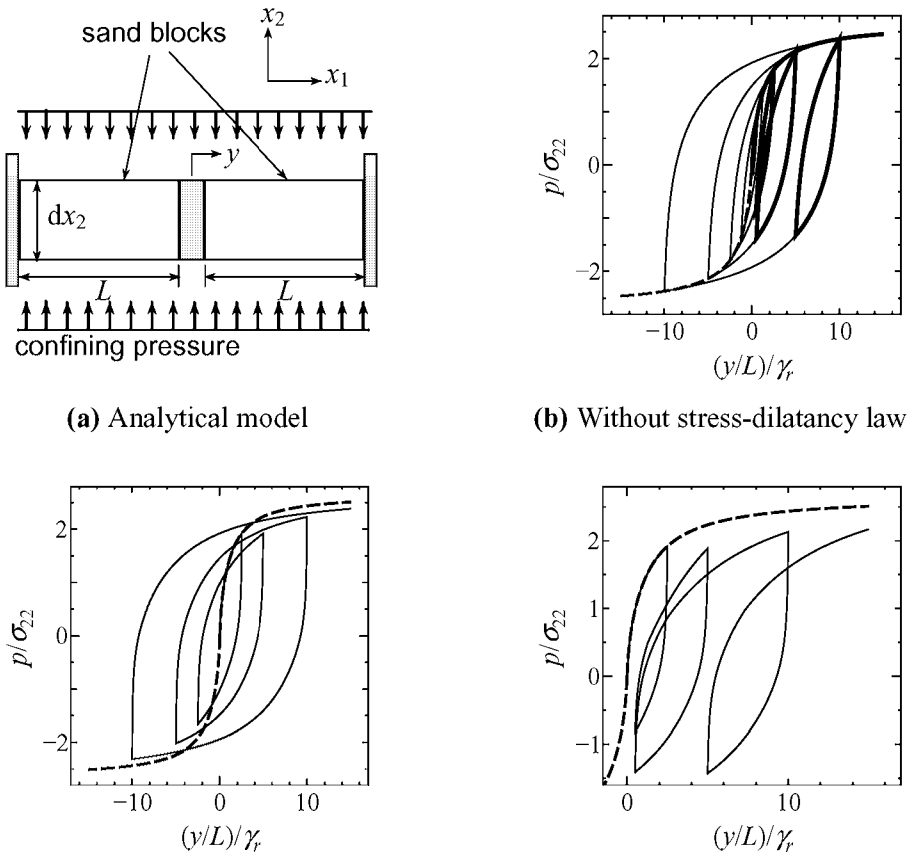

(a) Analytical model

(b) Without stress-dilatancy law

(c) With stress-dilatancy law

Figure 6 Analyses of the effects of the stress-dilatancy behavior of sand on p-y relations

teretic mechanism of $\sin\phi_{\mathrm{mob}}$-γ is presented by Masing's rule. In addition, we need to set a γ-$\varepsilon_{\mathrm{vol}}$ relation to describe the soil behavior under the plane strain condition. The following two cases are tested regarding the volumetric deformation component of the soil block in order to strengthen the contributions of the stress-dilatancy behavior.

1) Rowe's stress-dilatancy relation is adopted with the coefficient of dilatancy K of 3.5.
2) Instead of Rowe's stress-dilatancy law, $\varepsilon_{22} = \nu\varepsilon_{11}$ is used, where $\nu = 0.3$.

The former gives an instantaneous incremental dilatant strain depending on the current stress state, and the latter case has a stationary and reversible one-to-one relationship between ε_{11} and γ.

Figure 6 (b) shows the calculation results obtained without the stress-dilatancy law. The thin solid line shows a result for fully reversed cyclic loading, and the thick solid line shows a result for one-sided cyclic loading. On the other hand, presented in **Figure 6 (c)** are the results obtained considering the stress-dilatancy law. The left-hand graph in **Figure 6 (c)** shows a result for fully cyclic loading, and the right-hand graph shows a result for one-sided cyclic loading. The dashed lines show the corresponding monotonic loading results.

Only when the stress-dilatancy law is considered does the degradation from the monotonic loading curve appear. In particular, the p-y curve runs considerably lower than the previous peak states in the case of one-sided cyclic loading. When the surrounding soils undergo one-sided cyclic loading, large irreversible strain components appear in the soil

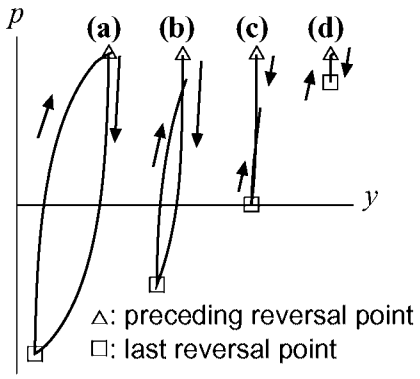

Figure 7 Degradation of p depending on the difference in the values of $|p|$ at the last and preceding reversal points

blocks at every cycle, making it difficult to recover the last soil resistance as mobilized in the previous loading cycle. Consequently, the stress-dilatancy behavior of sand is found to greatly affect the loading pattern dependency of the p-y relation.

Next, we assigned various y displacement histories to the model shown in **Figure 6 (a)** and obtained the p-y responses. Ultimately, the tendencies illustrated in **Figure 7** were observed. In one p-y cycle,

- the p-y curve returns to a point near the preceding reversal point when the intensities of $|p|$ are almost equal at the preceding and last reversal points (**Figures 7 (a)** and **(d)**).
- the p-y curve runs lower than the preceding reversal point with an increase in the difference in intensities of $|p|$ between the preceding and last reversal points (**Figures 7 (b)** and **(c)**).

A NEW NONLINEAR HYSTERETIC MECHANISM OF p-y

In this section, a new hysteretic mechanism of the p-y response is proposed. The new model will satisfy the characteristics as summarized in **Figure 7**. **Figures 8, 9, 10** and **11** illustrate the newly proposed hysteretic model. In order to facilitate the description for various conditions of nonlinear relations of p-y, we describe the hysteretic mechanism by means of combinations of piecewise straight branches.

We simplify the skeleton curve into a bi-linear curve of elastic and perfectly plastic type, as shown in **Figure 8**. It should be noted that the hysteretic mechanism, which will be proposed later, can be applied to any shape functions of the skeleton curve. In other words, we can use the combination of a curved skeleton curve and the newly proposed hysteretic mechanism.

The ultimate value p_U of p is provided by

$$p_U = \alpha_p K_P \gamma x_2, \tag{4}$$

where K_P is the passive earth pressure coefficient, γ is the soil weight per unit volume, x_2 is the depth, and α_p is a modification factor used to represent three-dimensional effects in the effective interaction zone in subsoil layers. The value of α_p in a subsoil layer can be

estimated through a load test on a single pile subjected to monotonic loading or fully reversed cyclic loading with a gradually increasing amplitude, or through a past theoretical study. For example, Kishida and Nakai (1979) have theoretically indicated mechanisms of plastic flow for surrounding soil in front of a horizontal loaded pile.

Based on a study by Kavvadas and Gazetas (1993) and Yoshida and Yoshinaka (1979), we express the subgrade reaction coefficient as follows:

$$k_H = \alpha_k k_0, \tag{5}$$

$$k_0 = (E_0/B_0) \times (B/B_0)^n, \tag{6}$$

where E_0 is the small strain deformation coefficient of soil, k_0 is the reference subgrade reaction coefficient, B is the width of foundation and is a diameter in the case of piles, B_0 is the reference width, and n is a constant value which represents the foundation width dependency of the subgrade reaction coefficient. In this paper, $B_0 = 0.3$ m and $n = -3/4$ are adopted in reference to the Japanese Specifications for Highway Bridges (Japan Road Association 2002) and Yoshida and Yoshinaka (1979). Here, α_k is a constant to fit the reference subgrade reaction coefficient with a bi-linear curve. It is assumed that the value of α_k is independent of depth. The values of α_k and α_p can be determined based on load tests on single piles subjected to monotonic loading or fully reversed cyclic loading.

The hysteretic mechanism in response to fully reversed loading, referred to herein as the Basic Hysteretic Mechanism, is a kind of peak oriented mechanism, as shown in **Figure 8**. A p-y curve runs toward a point corresponding to the ever-largest displacement $|y|_{\max}$. In addition, an unloading path bound for $p = 0$ from the last reversal point is regarded as a straight line with an unloading gradient of $k_{H\mathrm{unl}}$. $k_{H\mathrm{unl}}$ is provided by

$$k_{H\mathrm{unl}} = \beta k_0. \tag{7}$$

As shown by the pile experiments and the analyses using the sand block-rigid body-sand block model, the unloading rigidity can be assumed to be independent of the displacement level and loading history. We furthermore assume $\beta = 1$ in Eq. (7) since the unloading gradient is closely related to the unloading gradient of soil, which has the same order of small strain levels used to define k_0.

A point corresponding to the ever-largest displacement on the skeleton curve is referred to as a global control point C_i, where the suffixes i and j are 1 or 2 hereafter. A pair of global control points, C_1 and C_2, are located on the positive and negative sides, respectively, and are symmetric about the origin. For example, for the path e $\rightarrow$ f $\rightarrow$ g in **Figure 8**, $|y|_{\max}$ is the absolute value of the displacement amplitude of point 'e', $|y_e|$. The other global control point is defined as point 'g', i.e. $y_g = -|y|_{\max} = -y_e$. Furthermore, we refer to the curves connecting the global control points, C_i-C_j, as external curves. For simplicity in coding, internal curves that move inside the external curves are always bound for the last reversal point on the external curve or the outermost internal curve. We refer to the oriented points for this case as the local control points C_{Li}.

We then introduce a deterioration rule using target points. The deterioration rule is a special rule to account for the tendency shown in **Figure 7**. As demonstrated in **Figure 9**, a target point T_1 is defined as the intersection point of a reloading line with a gradient of k_{Hr}

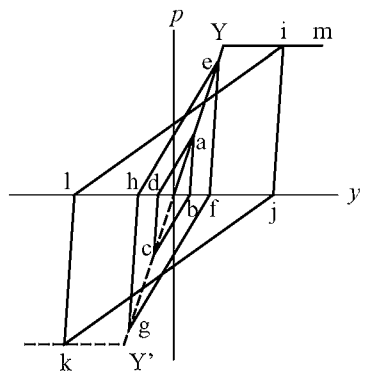

Figure 8 Basic Hysteretic Mechanism

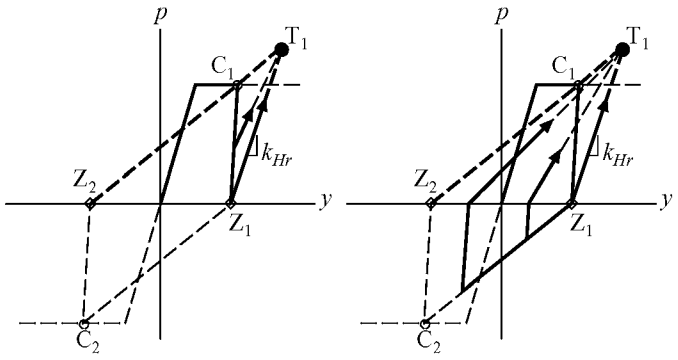

Figure 9 Deterioration rule

from the perfectly unloaded point Z_1 and an extension line of the external curve C_2-C_1 (i.e. Z_2-C_1), and we further assume that the path after a reversal on the external curve C_1-C_2 is always bound for the target point T_1.

In the right-hand diagram of **Figure 9**, the curve after the last reversal is made up of an unloading branch with the gradient of $k_{H\text{unl}}$ and the subsequent reloading branch bound for T_1. The other target point T_2 can be derived in the same manner by using the perfectly unloaded point Z_2 from the global control point C_2, the gradient k_{Hr}, and the extension line of the corresponding external curve C_1-C_2 (i.e. Z_1-C_2).

We refer to the line connecting the perfectly unloaded point Z_i to the target point T_i as a reference reloading line and its gradient k_{Hr} as the reference reloading gradient. The reference reloading gradient is expressed as

$$k_{Hr} = Mk_{H\text{unl}}, \tag{8}$$

where M is a constant. The value of M is not larger than one and is satisfied by the condition whereby the extensions of the reference reloading curve and the external curve must possess a cross point in the first or third quadrant for T_1 or T_2, respectively. When an interaction spring is subjected to fully reversed cyclic loading, no deterioration of p appears, regardless of the value of M. When $M = 1.0$, the hysteretic mechanism becomes identical to the Basic Hysteretic Mechanism. The value of M could be chiefly related to the density of sand, since the degree of the dilatancy deformation of sand depends considerably on the density.

As shown in **Figure 10**, when a p-y curve crosses an external curve (for example, C'_1-Z'_1-C'_2 in **Figure 10**) and changes the traveling direction, the global control points C'_1 and C'_2 are renewed to C_1 and C_2. In **Figure 10**, the prime denotes the points before the renewal. As shown in **Figure 10**, C_i must be set as the intersection of the skeleton curve to a line passing through the reversal point and having a gradient of $k_{H\text{unl}}$ when all points must be updated and the reversal point is not on the skeleton curve. Together with the update of C_1 and C_2, external curves and points Z_1 and Z_2 are updated, and the target points T_1 and T_2 are then redefined as shown in **Figure 10**.

A schematic diagram showing the behavior of internal curves is presented in **Figure 11**. Internal curves always orient toward a local target point T_{L1} or T_{L2} depending on the traveling direction. A local target point, T_{Li}, is set on either the intersection of the local

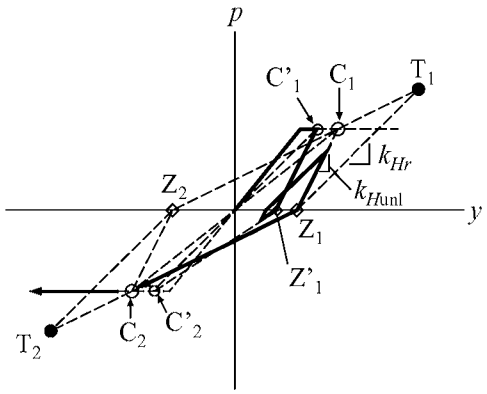

Figure 10 Updating of points C_i, Z_i, and T_i

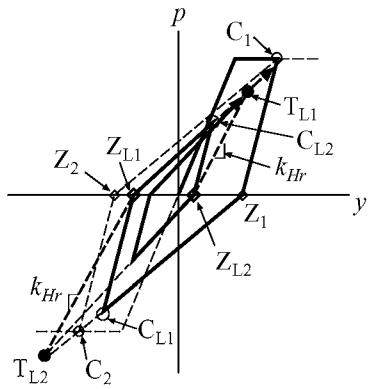

Figure 11 Behavior of internal curves

reference reloading line and the outermost internal curve or the extension thereof, or the intersection of the local reference reloading line and the external curve or the extension thereof, where the local reloading line is a line starting from point Z_{Li} and having the gradient of k_{Hr}, and the point Z_{Li} is the perfectly unloaded point from the reversal point on the outermost internal curve or an external curve. If an internal p-y path reaches Point T_{L1} in **Figure 11**, the path then runs along the intercepted outermost internal curve bound for the skeleton curve and then moves along the skeleton curve. When a displacement reversal takes place after an internal path crosses the curve C_{Li}-Z_{Li}, the corresponding local control point C_{Li}, point Z_{Li}, and local target point T_{Lj}, are renewed in the same manner as the global control points.

NUMERICAL SIMULATION USING THE PROPOSED HYSTERETIC MECHANISM

In order to check the validity of the proposed model, the pile load experiments presented above are numerically simulated using the proposed model. Case S1 experiment, involving a fully reversed cyclic load, and Case S3 experiment, involving a one-sided cyclic load, are examined. A beam-on-nonlinear-Winkler-foundation model is used here with the proposed hysteretic mechanism of the Winkler spring. Piles are dealt with as beams and are modeled using beam elements. Nonlinearity in the bending behavior of a pile is considered by a typical elasto-perfectly plastic bi-linear relation of moment versus curvature, where the work hardening and the Bauschinger effect are ignored. The elastic gradient is given by the flexural rigidity, and the ultimate bending moment is set as the plastic moment of the cross section. The bottoms of the piles were connected by the hinge boundary condition in the numerical simulation, so that the horizontal and vertical displacements are fixed at the bottom, while rotation is free.

Distributed lateral Winkler springs are integrated into discrete lateral springs at finite element nodes. The load-displacement relationship of each integrated lateral spring is obtained based on the p-y relationship at a depth of the middle point of the beam element. We derived the value of E_0 at each depth using $E_0 = 2(1 + \nu)G_0$, based on the value of G_0 shown in Eq. (1), which is obtained by cyclic triaxial compression tests of sand. σ'_c is replaced by a mean effective stress estimated by $\sigma'_m(x_2) = (1 + 2K_0)\sigma'_v(x_2)/3$ (kN/m^2), where $\sigma'_v(x_2)$ is

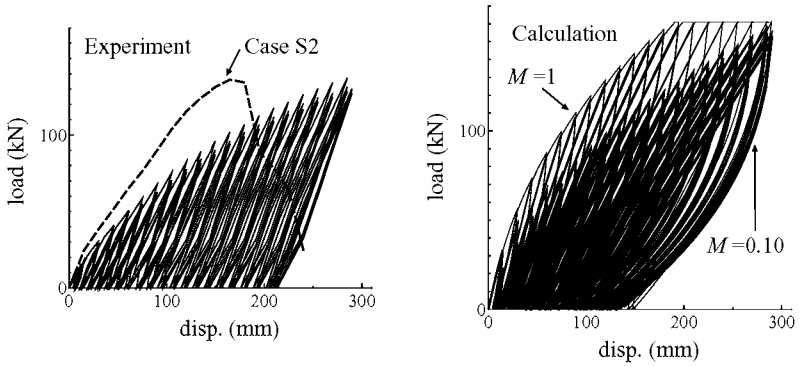

Figure 12 Load-displacement relations at the loading point (Case S3)

an effective overburden stress at depth x_2. Here, K_0 is the coefficient of earth pressure at rest and is estimated by a typical empirical equation $K_0 = 1 - \sin\phi'$. For simplicity, the value of Poisson's ratio, ν, is set equal to 0.5 without any physical consideration.

We should first determine the values of parameters α_p and α_k in Eqs. (4) and (5) for the skeleton curves of the p-y relations. The experimental results for Case S1 are used to estimate the values of α_p and α_k, since we can regard the envelope curve of the relationship of horizontal load and horizontal displacement at the loading point equivalent to that in a monotonic loading condition. Parametric monotonic analyses were carried out using pairs of values of parameters α_k and α_p, and the calculated monotonic load-displacement curves at the loading point were compared with the skeleton curve of the load-displacement curve observed in the experiment. Finally, $\alpha_p = 4.0$ and $\alpha_k = 0.1$ were chosen for any depth. The maximum soil resistances p_U obtained by the present method with $\alpha_p = 4.0$ are very close to theoretical solutions given by, for example, Kishida and Nakai (1979). This finding supports the feasibility of a theoretical prediction of the maximum soil resistance, even in the framework of the present hysteretic mechanism of p-y.

We then carry out back analyses using various values of M for the Case S3 experiment in order to select a suitable value of M that specifies the deterioration of p for a cyclic loading on one-side. Calculated and measured load-displacement curves at the point of loading are shown in **Figure 12**, where the skeleton curve of the experimental results for Case S2 is also shown for comparison. Note that the proposed hysteretic mechanism with $M = 1$ is equivalent to a typical peak-oriented bi-linear mechanism without the deterioration that normally occurs with fully reversed cyclic loading. The use of $M = 1$ overestimates the load, and the results are similar to the experimental results for Case S2, in which the pile was subjected to fully reversed cyclic loading. A value of $M = 0.10$ provides the best match calculation result regarding the skeleton curve of the load-displacement relationship.

A comparison of calculated p-y relations is shown in **Figure 13** along with the experimental results. The proposed p-y mechanism when $M = 0.1$ is used is able to reasonably capture the observed load transfer between soil and pile. Note that the p-y curves are shown up to a displacement level of 6δ since the pile remained within the elastic range in the experiment.

When a combination in numerical parameters of $\alpha_k = 0.10$, $\beta = 1.0$ and $M = 0.10$ is assumed, the initial gradient of the skeleton curve, k_H, given by Eq. (5), and the reference

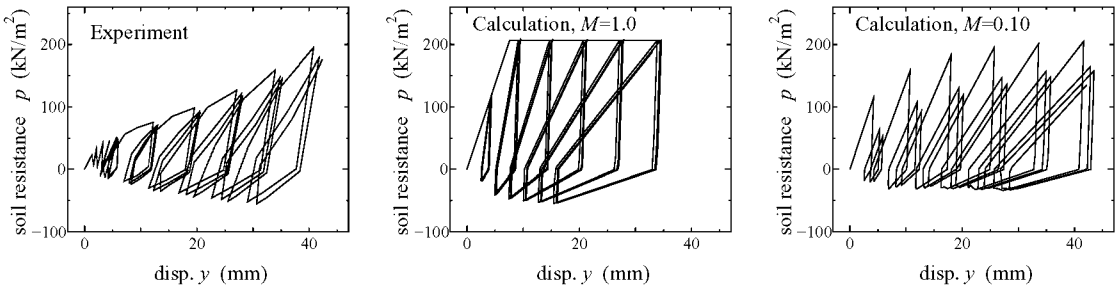

Figure 13 p-y relations (Case S3, GL −0.96 m, up to the 6δ cycle)

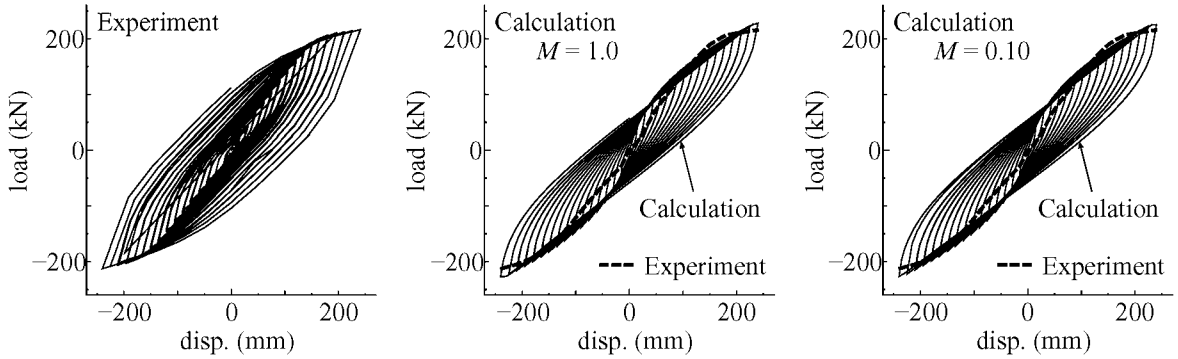

Figure 14 Comparison of calculated load-displacement curves at the loading points of M = 1 and M = 0.10 with the experimental result (Case S1)

reloading gradient, k_{Hr}, provided by Eq. (8), become identical. This fact is quite interesting, and the values of k_H and k_{Hr} might have the same order in general. The skeleton curve of p-y would be apparently shifted due to the difference in the residual strain of the surrounding soil on the both sides with respect to the pile, depending on loading pattern.

The proposed hysteretic mechanism of p-y should respond in an equivalent manner, being independent of the value of M in the case of fully reversed cyclic loading. **Figures 14** and **15** compare the experimental results for Case S1 to the numerical results calculated using the proposed hysteretic mechanism with M = 1 and 0.10. In **Figure 14**, the dashed lines show the experimental envelope curve for comparison. Discrepancies in the calculated results due to differences in M were barely discernible, and the calculated results show good agreement the experimental results. This demonstrates that the proposed hysteretic mechanism works as expected.

CONCLUDING REMARKS

We proposed a new hysteretic mechanism of p-y and introduced a target point to account for the loading pattern dependency of p-y. The authors argue that the consideration of the loading pattern dependency of p-y in dynamic analyses in deep foundations is essential in situations such as when the foundations of retaining structures are subjected to earthquakes, or when severe eccentric motion appears due to P-Δ effects caused by the plasticization of a pier or a structural member of a foundation. The principle of the proposed mechanism is confirmed through horizontal cyclic pile load experiments and through the general behavior

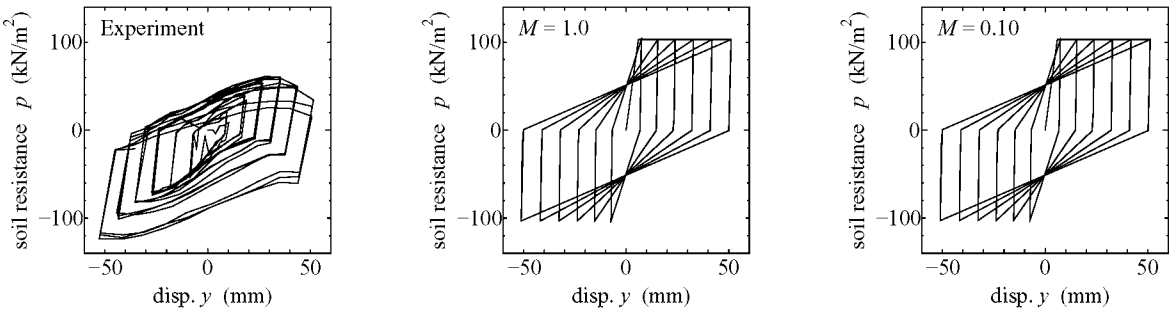

Figure 15 Comparison between the calculated p-y curves of $M = 1$ and $M = 0.10$ and the experimental results (Case S1, GL −0.48 m, up to the 6δ cycle)

of sand in the deformation mode of cyclic compression-extension loading generated in the near-field soil during earthquakes. The beam-on-nonlinear Winkler spring model with the proposed hysteretic mechanism of p-y can be considered to reasonably reproduce the nonlinear soil-pile interaction under seismic random loading during large earthquakes without resorting to a sophisticated method such as three-dimensional finite element analysis and can be easily applied, even in practical design.

Acknowledgment The authors would like to thank Prof. Fumio Tatsuoka of Tokyo University of Science for his valuable suggestions and for providing experimental data for sand subjected to cyclic compression-extension deformation in the plane strain condition.

References

Fukui, J., Y. Kimura, M. Ookoshi, and A. Banno (1998). Large scale experimental study on horizontal restoring forces of single piles in sand. *Technical Memorandum of PWRI, Public Works Research Institute* (3552). In Japanese.

Japan Road Association (2002). *Specifications for Highway Bridges, Part IV, Substructures*. Tokyo: Maruzen. In Japanese.

Kavvadas, M. and G. Gazetas (1993). Kinematic seismic response and bending of free-head piles in layered soil. *Geotechnique 43*(2), 207–222.

Kishida, H. and S. Nakai (1979). Analysis of a laterally loaded pipe with non-linear subgrade reaction. *Trans. of A.I.J.* (281), 41–53. In Japanese, with English summary.

Masuda, T., F. Tatsuoka, S. Yamada, and T. Sato (1999). Stress-strain behaviour of sand in plane strain compression, extension and cyclic loading tests. *Soils and Foundations 39*(5), 31–45.

Yoshida, I. and R. Yoshinaka (1979). A method to estimate modulus of horizontal subgrade reaction for a pile. *Soils and Foundations 12*(3), 1–17.